19951402

N95- 20508

CHEMICAL BEAM EPITAXY FOR HIGH EFFICIENCY PHOTOVOLTAIC DEVICES

A. Bensaoula, A. Freundlich, M.F. Vilela, N. Medelci, and P. Renaud
University of Houston
Houston, Texas

INTRODUCTION

InP-based multijunction tandem solar cells show great promise for high conversion efficiency (η) and high radiation resistance. InP and its related ternary and quaternary compound semiconductors such as InGaAs and InGaAsP offer desirable combinations of energy bandgap values which are very suitable for multijunction tandem solar cell applications. The monolithically integrated InP/$In_{0.53}Ga_{0.47}As$ tandem solar cells are expected to reach efficiencies above 30%. Wanlass et al. (ref. 1) have reported AM0 efficiencies as high as 20.1% for two terminal cells fabricated using atmospheric-pressure metalorganic vapor phase epitaxy (APMOVPE). The main limitations in their technique are first related to the degradation of the intercell ohmic contact (IOC), in this case the $In_{0.53}Ga_{0.47}As$ tunnel junction during the growth of the top InP subcell structure, and second to the current matching, often limited by the $In_{0.53}Ga_{0.47}As$ bottom subcell.

Chemical beam epitaxy (CBE) has been shown to allow the growth of high quality materials with reproducible complex compositional and doping profiles. The main advantage of CBE compared to metalorganic chemical vapor deposition (MOCVD), the most popular technique for InP-based photovoltaic device fabrication, is the ability to grow high purity epilayers at much lower temperatures (450°C - 530°C) (ref.2). In a recent report Yamaguchi et al (ref.3) have shown that cost-wise CBE is a breakthrough technology for photovoltaic (PV) solar energy applications. Through the research effort undertaken in our laboratory, we have seen a rapid progress in the energy conversion efficiency of InP-based solar cells fabricated using chemical beam epitaxy (ref.4). This communication summarizes our recent results on PV devices and demonstrates the strength of this new technology.

GROWTH TECHNIQUE

The realization of high performance solar cells and tunnel junctions requires extremely high purity layers, perfect control on hole and electron concentrations as well as low interdiffusion of dopant species across the junction during the device growth procedure. Therefore, a relatively low temperature growth process and a good control of the interface properties are required. CBE meets the above requirements since high quality GaAs, InP, GaP, InAsP, GaInP and InGaAs layers can be grown at lower temperatures than those used in more conventional techniques such as LPE, MOCVD, and even MBE. Moreover, it combines features from both MOCVD and MBE, allowing the growth of semiconductor heterostructures with monolayer abruptness and thickness control as well as easy multiwafer scale-up.

We have already demonstrated, using CBE, the growth of a variety of high quality heterostructures ranging from lattice matched (InGaAs/InP) and strained (InAsP/InP) to highly stained InAs/InP (ref. 5). In these studies the effect of growth temperatures and interruption schemes at the interfaces was demonstrated to be crucial. To illustrate the growth control capability of CBE we mention here our group latest results in the fabrication of perfectly balanced highly strained heterostructures GaP(under tension)/GaAs/InP (under compression) superlattices with thicknesses up to 1 μm (ref.6). These heterostructures are highly ordered and show very low defect densities as seen in Figure 1. High resolution x-ray diffraction (400) from these layers exhibit a residual strain of less than $8x10^{-5}$; by comparison residual strain in GaAs/AlAs structures is $1.38x\ 10^{-3}$.

CBE's flexibility in allowing the growth of such high quality complex heterostructures permits the implementation of novel PV design concepts with expected higher efficiencies at no added fabrication costs (sometimes lower). As an example we are investigating the use of internal Bragg reflectors and the addition of MQWs in a standard diode structure to enhance the photon absorption and increase the cell photocurrent, thus significantly improving the PV

efficiency. Preliminary results on adding MQWs in the intrinsic region of a P-I-N structures are very encouraging and will be published elsewhere.

All our Epitaxial growth runs were accomplished in a Riber CBE 32 system using trimethyl-indium (TMI), triethyl-gallium (TEG) and pre-cracked arsine (AsH_3) and phosphine (PH_3) as growth precursors. While research to date has included the growth of InP-based PV devices on both GaAs and GaAs/Si, we will restrict ourselves in this paper to homoepitaxial growths on InP substrates (mainly InP:S (100)). Reflection high energy electron diffraction (RHEED) was used to monitor the surface morphology during the growth process as well as calibrate an optical pyrometer focused on the substrate. This calibration uses the oxyde desorption temperature (517 ^{o}C) as the reference point. When this temperature is reached, the RHEED pattern changes from diffuse bulk type spots to clear bright lines. Due to the strong dependence of the InGaAs alloy composition on the substrate temperature, lattice matching with respect to InP was studied in the 450-530 ^{o}C temperature range. Lattice matching to better than 10^{-3}, as checked by High Resolution Double Crystal X-ray Diffraction, was achieved reproducibly, demonstrating excellent composition control for our ternary compounds.

DOPING STUDIES

Both the Be and Si doping behavior of InGaAs layers fabricated on InP:Fe (100) semi-insulating substrates at relatively low temperatures (450 ^{o}C to 480 ^{o}C) were investigated. Be and Si dopings were achieved using solid source effusion cells. Doping studies were carried out in lattice matched conditions. Be doped p-InGaAs with net hole concentrations (as determined from Hall measurements) varying from $2x10^{17}$ cm^{-3} to $2x10^{20}$ cm^{-3} were achieved. No surface degradation was observed, even at doping levels as high as $2x10^{20}$ cm^{-3}. Si doping was investigated within a doping range of 10^{17} cm^{-3} to $2x10^{19}$ cm^{-3}. No noticeable electrical compensation was detected and good reproducibility was achieved from run to run.

In order to investigate the cross-diffusion behavior and to further assess the cross-doping profiles, Secondary Ion Mass Spectroscopy (SIMS) experiments were carried out on InGaAs multilayered structures fabricated with a combination of different Be and Si doping levels and undoped spacers. SIMS experiments were performed in a Cameca IMS 4F system and both O^{+} and Cs^{+} profiles were taken for Be and Si respectively. Figure 2 represents compilation of O^{+} and Cs^{+} SIMS data. As it can be observed, the memory effects are in the range of 10^{16} cm^{-3} or less for both Be and Si doping. Furthermore, at the interface between Be and Si doped layers, observed cross-diffusions are within the experimental error. The sharp diffusion profiles between Be and Si are consistent with solar cells and tunnel junctions low inter-diffusion requirements. Our results indicate that p/n or n/p structure should exhibit similar behavior. We have chosen deliberately to study p/n type devices.

SOLAR CELL AND TUNNEL DIODE DEVICES

Figure 3 shows a diagram of a tandem solar cell structure. Besides achieving the proper electrical and structural quality for the individual layers, two issues stand out in the realization of these devices. The first relates to the fabrication of thin tunnel junctions with high current carrying capabilities and minimum resistivities. The second concerns the ability to grow a high quality InP solar cell on InGaAs at low enough temperature so as to preserve the characteristics of the underlying tunnel junction. Following we will describe the growth and fabrication of the individual tandem components.

$In_{0.53}Ga_{0.47}As$ solar cell

The cell fabrication process begins with the CBE growth of a structure as shown in Figure 3 (bottom cell). A summary of the characteristics under natural sunlight and without anti-

reflection coating is: J_{SC}=30mA/cm^2; V_{OC}=0.27V; FF=57.8%; η=5.1%, for an incident sunlight power of 91.4mW/cm^2. A double anti-reflection coating (ZnS/MgF_2) was deposited and the new electrical characteristics under natural sunlight are (Figure 4): J_{SC}=60mA/cm^2; V_{OC}=0.295V; FF=54.2%; η=10.2%, for an incident sunlight power of 94.2mW/cm^2 (total area, 0.25cm^2). In this particular sample we note that a strong increase in the photocurrent after anti-reflection coating is observed. This increase cannot be explained solely by the addition of the anti-reflection layer. It is believed that this diode had a much lower shunt resistance before the dielectric deposition. A leakage current prior ARC coating was responsible for the lower photocurrent measured. Similarly after ARC the fill factor (FF) is smaller, a result of a higher series resistance.

The Spectral Response (SR) characteristics after ARC of this InGaAs cell are presented in Figure 5. A minimum at 680nm is clearly observed. This minimum is related to reflections at the InP window layer (we remind the reader that the ARC is optimized for the InGaAs material). We note that for wavelengths higher than 1100nm, the SR decreases noticeably, a result of a non optimized base layer. Both the base layer thickness and the minority carrier lifetime in this layer must be investigated to better understand the cause for this decrease. The high response at smaller wavelengths shows however the high quality of the emitter layer. In conclusion, while further improvements in the cell characteristics are expected through a better optimization of the base layer, the high photocurrent density already demonstrated in these cells (**60mA/cm^2**, the highest ever reported) is very promising.

The dark I-V and short circuit current (I_{SC}) as a function of the open circuit voltage (V_{OC}) characteristics have been measured as well. The shunt resistance (R_{Sh}) from dark I-V, the diode ideality constant (n) from I_{SC}-V_{OC} and the saturation current (J_S) from I_{SC}-V_{OC} were calculated. These values are shown in Table I. An ideality constant of 2.2 is expected for a small bandgap diode such as InGaAs. Both the shunt resistance (42 Ω*cm^2) and the saturation current (J_S = 0.6 mA/cm^2) can be improved through proper mesa passivation.

InP solar cell

Figure 3 shows the doping levels and thicknesses for the InP solar cell (top cell). Its electrical characteristics are shown in Figure 6. The characterization results performed under natural sunlight without anti reflection coating are: J_{SC} = 20 mA/cm^2, V_{OC} = 0.82 V, FF = 77%, and η=13%, for an incident sunlight power of 97 mW/cm^2. After the antireflection coating this solar cell presents 18% conversion efficiency under solar simulator. Its spectral response is shown in Figure 5. The flat SR from 450nm to 850nm shows the high quality of this material. The lower efficiency at smaller wavelengths (<400nm) is expected since this InP solar cell does not have any window layer. By using a window layer or decreasing the emitter thickness it is possible to improve the SR at lower wavelengths. In Table-1 the R_{Sh}, I_S and n for this solar cell are given. It is expected that R_{Sh} and the InP solar cell efficiency will increase after mesa passivation. A mesa passivation and a window layer should further increase the efficiency to 22%.

$In_{0.53}Ga_{0.47}As$ tunnel junction

p^+/n^+ $In_{0.53}Ga_{0.47}As$ tunnel junction structures with different active layer thicknesses (ranging from 0.2 to 0.8 μm) and growth temperatures (450-530 ^{0}C) were grown. Devices were made using a standard wet etching process with mesa openings of 100 and 200 μm in diameter. Evaporated Au was used for front and back contacts. No high temperature annealing of the metallic contact layers was performed.

The net carrier concentrations as extrapolated from Hall measurement data for devices discussed here were varied from $N_A=1.3x10^{19}$ to $N_A=5x10^{19}$ cm^{-3} in the p-type layers, and from $N_D=7x10^{18}$ to $N_D=1.3x10^{19}$ cm^{-3} in the n-type layers. Thus, junctions with highly degenerate n type sides (> 10 kT) and degenerate p type sides (> kT) were obtained, resulting in devices with effective dopings $N^*=N_AN_D/(N_A+N_D)$ ranging from $5.9x10^{18}$ to $8.3x10^{18}$ cm^{-3}.

All our devices exhibit excellent I-V characteristics. Peak current densities obtained in this work are among the highest ever reported for epitaxial tunnel junctions. The best room temperature peak current density exceeds 1000 A/cm^2 (Figure 7); and specific resistivities lower than 10^{-4} $\Omega.cm^2$ were measured. Maximum resistivities R_{max} (peak current to peak voltage ratios) are in the $2x10^{-4}$ to $5x10^{-4}$ $\Omega.cm^2$ range, making these junctions highly suitable as IOCs for the InP/InGaAs tandem solar cell. High peak to valley ratios are exhibited by many devices with room temperature peak to valley ratios of 9 and peak current densities greater than 550 A/cm^2.

In order to investigate the evolution of the tunnel junction properties when incorporated in the InP/InGaAs tandem solar cell structure, an InGaAs tunnel junction with an effective doping of $7x10^{18}$ cm^{-3} was subjected to the growth of a thick (>3 μm) InP solar cell. Prior to the solar cell growth, the tunnel junction coated wafer was cut in two pieces. One piece was processed as a reference sample. The InP solar cell regrowth structure was realized with standard parameters (doping and layer thicknesses) on the second piece of the wafer (ref. 7). Following the growth process, the InP solar cell was selectively etched using a HCl solution and mesa processing was accomplished. Even after more than 2 hours at 560 ^oC, no degradation of the tunnel junction characteristics is observed. The device still exhibited very high peak current densities, up to 860 A/cm^2 as shown in Figure 8. Hence, our tunnel junctions are suitable for use in tandem structures either in a planar or the more demanding patterned electrical interconnect concept (ref. 8). With the above characteristics (tunneling currents and resistivities), the voltage drop accross a patterned tunnel junction aligned with the top solar cell grid (e.g. 5% shadowing) at concentration of 100 x AM0 will be below 10^{-2} volts.

InP/InGaAs tandem solar cell with planar tunnel diode

A complete structure similar to that shown in Figure 3 was grown. In the following case the IOC for the tandem is realized with a planar tunnel diode. A very low photocurrent output for these type of structures under natural sun light illumination is characteristic. In Figure 9 we shown the electrical characteristics of this tandem under concentrated light stimulation. The tandem's V_{OC} is equal to the sum of that from the InGaAs botton cell (V_{oc1}) and that from the InP top cell (V_{OC2}) - $V_{OC} = V_{oc1} + V_{oc2} = 1.2$ V)-. The SR was performed in order to investigate its low photo sensitivity (Figure 10). Despite the low overall photocurrent ouput, the InP top cell has a relatively good response. While the tandem responds fairly well for wavelenghts less than 920 nm, for photons with wavelengths between 920nm and 1650nm the SR is near zero. As expected the 0.2μm thick IOC tunnel diode absorbs nearly all the incoming photons thus totally blocking the irradiation of the bottom cell. The implications of this result is either the adoption of a tandem cell structure using a patterned tunnel concept, as proposed by Shen et al (ref. 8), or the use of ultra thin (~400Å) planar tunnel diodes. Both of these concepts are possible using CBE and are currently being investigated.

InP/InGaAs tandem solar cell with patterned tunnel diode

A structure similar to that of Figure 3 was grown but this time in a two-step process. First, the growth of the InGaAs solar cell followed by the InGaAs tunnel diode was performed. The sample was removed from the growth chamber and the tunnel diode was patterned with the same mask as the contact grid. Then, the sample was reloaded into the CBE chamber and the

InP solar cell was grown on top. Figure 10 shows the SR (after anti-reflection deposition) of this tandem. We see a noticeable improvement in the tandem photoresponse. The tunnel diode patterning has allowed a much higher illumination of the bottom cell. The InGaAs bottom cell however displays a higher SR compared to that of the InP top cell. This is mainly due to inhomogeneous etching during the patterning step and regrowth issues resulting in an inhomogeneous and poor quality InP material in the top cell. Nevertheless under light stimulations the patterned tunnel diode shows low resistivity and the tandem I-V characteristics display good ohmic IOC behavior even for high polarization. It is clear that regrowth procedures optimization will be necessary.

CONCLUSION

Chemical beam epitaxy has been shown to allow the attainment of high quality InGaAs and InP layers. InP and InGaAs solar cells have been obtained with high efficiency photoconversion, 10.2% for InGaAs solar cell and 18% for InP solar cell. The tunnel diodes obtained with this technique have very high peak current densities and show to be thermically stable during the top cell growth. This realization has permitted the fabrication of monolithically integrated tandem solar cells. The planar tandem device exhibits an open-circuit voltage equal to the sum of that of the individual sub-cells (Voc = 1.2 V) demonstrating negligible voltage drop at the interconnect, but the InGaAs tunnel diode was shown to absorb highly thus blocking irradiation of the InGaAs bottom cell. By using patterned tunnel junctions we observe a significant improvement in the tandem photoresponse, but a lower spectral response for the top InP cell. Work underway is focusing on optimization of the regrowth procedures to address this problem.

** *Present address LPSES - CNRS, Valbonne - 06560 - France*

REFERENCES

1. M. W. Wanlass, J. S. Ward, K. A. Emery and T. J. Coutts; Proc. 23rd IEEE -PV Conf.; 1993; pp 621.

2. A. Freundlich, M. F. Vilela, A. Bensaoula, and N. Medelci; Proc. 23rd IEEE -PV Conf.; 1993; pp 644.

3. M. Yamaguchi, T. Warabisako and H. Sugiura, Journal of Crystal Growth; 136; 1994; pp.29.

4. A. Bensaoula, N. Medelci, M. F. Vilela and A. Freundlich; 6th International Conference on InP and Related Materials; Santa Barbara - CA - USA ; IEEE catalog #94CH3369-6, (1994), pp.280.

5. V. Rossignol, A. Bensaoula, A. Freundlich, and A. H. Bensaoula; 5th International Conference on InP and Related Materials; Paris - France ; IEEE catalog #93CH3276-3, (1993), pp.127.

6. A. H. Bensaoula, A. Freundlich, A. Bensaoula, V. Rossignol and A. Ponchet; J. Vac. Sci. Technol. B 12(2), 1994, pp. 1110.

7. A. Freundlich, M. F. Vilela, A. Bensaoula, and N. Medelci, Proc. 23th IEEE-PV Conf., 1993, pp. 644.

8. C. C. Shen, P. T. Chang and K. A. Emery; Proc. 22nd IEEE -PV Conf.; 1991; pp 381.

*This work was supported by the state of Texas advanced technology program 93-03652-260 , 93-003652-236 and 91-03652-243 and advanced research program 93- 003652-224 and partially supported by IST Inc. The authors would like to thank A. H. Bensaoula, E. Kim and V. Rossignol for their help in this project.

TABLES

Table I. - Shunt Resistance (R_{sh}), Saturation Current (J_s) and Ideality Constant (n) for the solar cells studied in this work.

Sample	InGaAs	InP	Patterned tandem	Planar tandem
R_{sh} ($M\Omega^*cm^2$)	$4.2x10^{-5}$	0.25	$1.2x10^{-3}$	2
J_s (mA/cm^2)	0.6	$8x10^{-9}$	0.7	$8x10^{-4}$
n	2.2	1.65	—	—

FIGURES

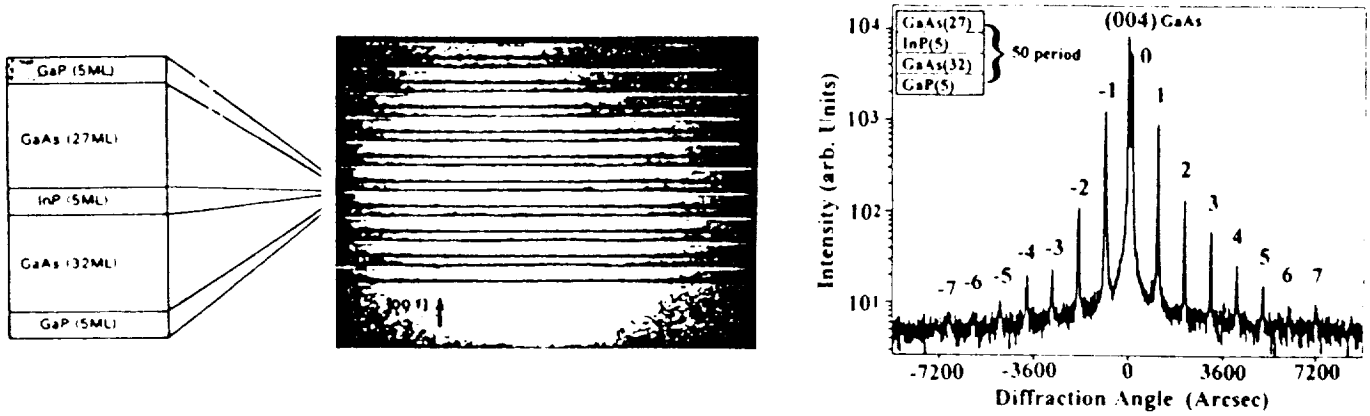

(a) (b)

Fig. 1 - GaP/GaAs/InP superlattice, a 50-period GaP(5ML)/GaAs(32ML)/InP(5ML)/GaAs(27ML), (a) cross-sectional TEM and (b)High resolution x-ray diffraction patterns (ref. 6).

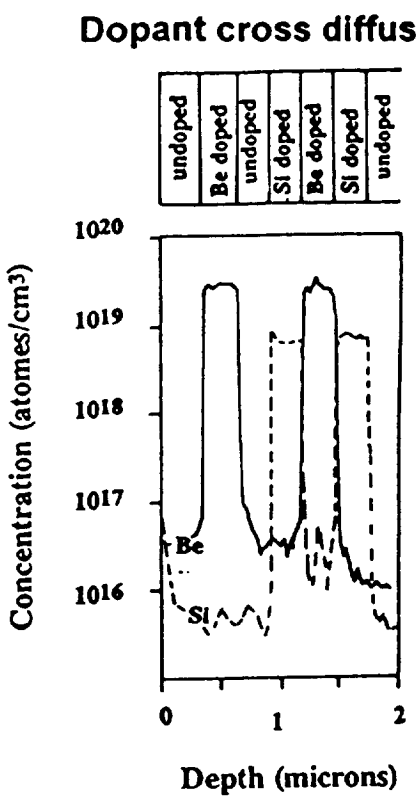

Fig. 2 - Secondary Ion Mass Spectroscopy of alternated dopant layers (Be and Si) and undoped spacers.

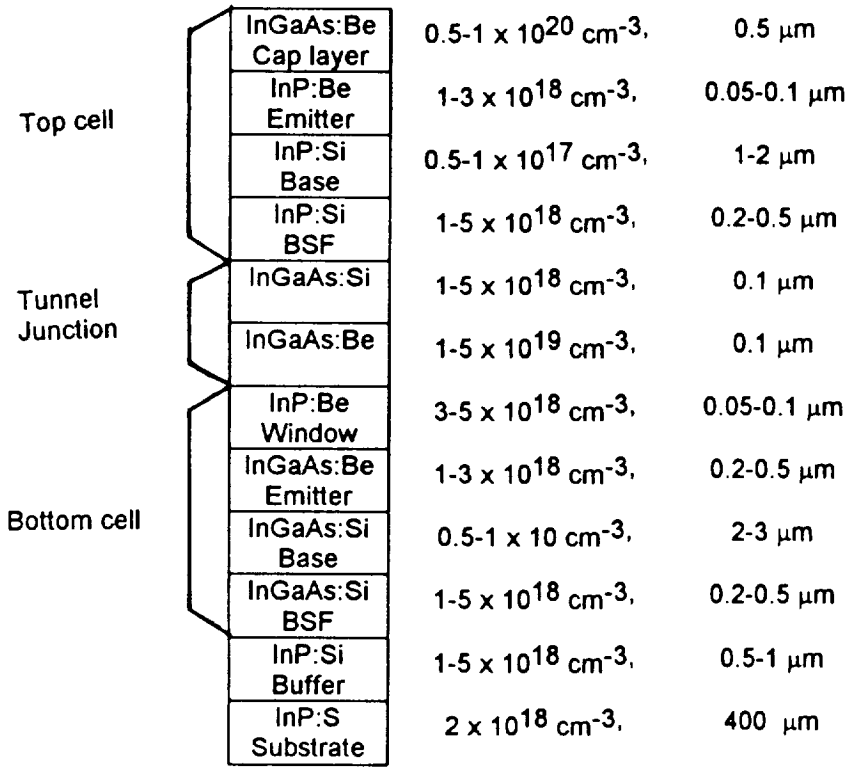

Fig. 3 - InP/InGaAs tandem solar cell structure. Doping levels and thicknesses are shown.

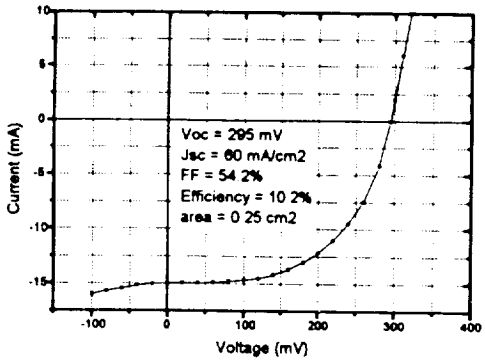

Figure 4 : Electrical characteristics of the InGaAs solar cell under natural sunlight, with anti reflection coating.

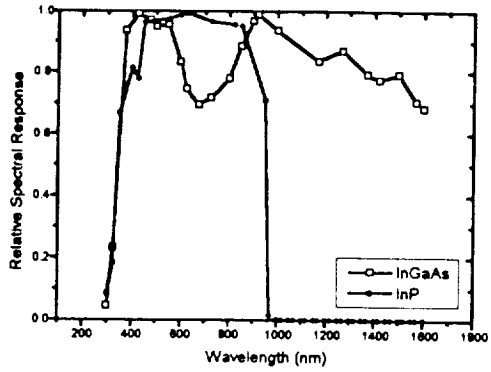

Figure 5 : Spectral Response of the InGaAs solar cell (opened squares) and InP solar cell (solid circles).

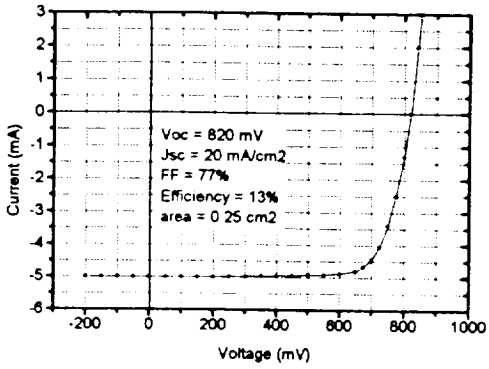

Figure 6: Electrical characteristics of the InP solar cell under natural sunlight (without anti reflection coating).

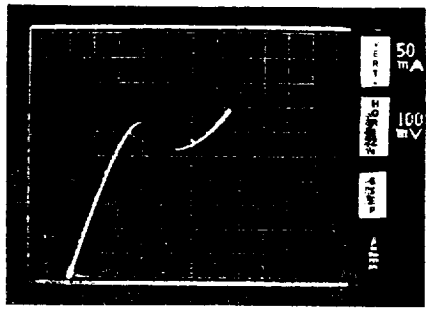

Figure 7: Room temperature I-V characteristics of InGaAs tunnel junction (mesa diameter = 200 μm) with a peak current of 1015 A/cm^2.

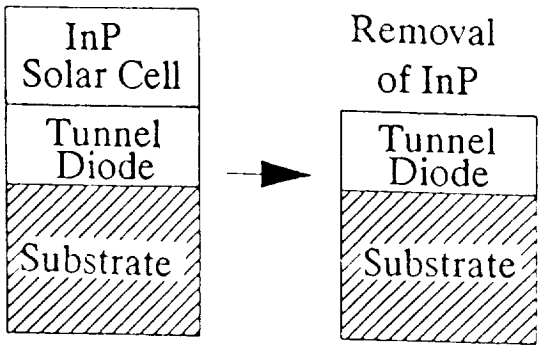

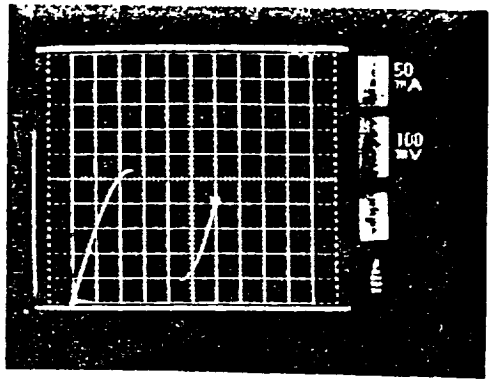

Figure 8: I-V characteristic of a InGaAs tunnel junction (mesa 200 μm in diameter) after solar cell growth. J_p = 860 A/cm^2, R_{max} = 2.9 x 10^{-4} Ω.cm^2.

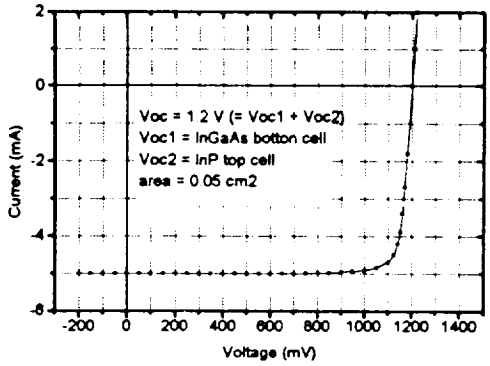

Figure 9 : Electrical characteristics of the tandem solar cell with a planar tunnel diode under concentrated light stimulation.

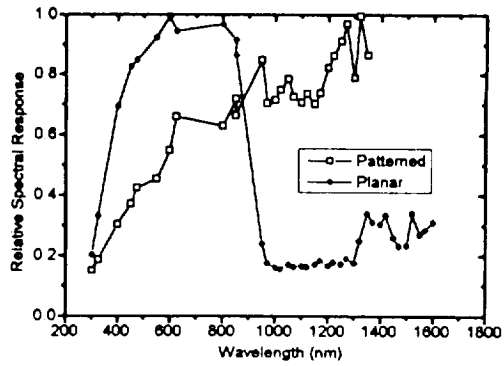

Figure 10 : Spectral Response of the InGaAs/InP tandem solar cell with a planar tunnel diode (solid circles) and InGaAs/InP tandem solar cell with a patterned tunnel diode (opened squares).